Available online at website: https://journal.bcrec.id/index.php/bcrec

Bulletin of Chemical Reaction Engineering & Catalysis, 21 (2) 2026, 385-402

Original Research Article

Efficient Adsorption of Tetracycline from Aqueous Solution onto Zinc Oxide Nanoparticles: Isotherm, Kinetic, Regeneration and Thermodynamic Studies

Zahraa A. Abd Almjeed*, Ahmed A. Mohammed

Department of Environmental Engineering, College of Engineering, University of Baghdad, Iraq.

Received: 7th December 2025; Revised: 11th February 2026; Accepted: 13th February 2026
Available online: 28th February 2026; Published regularly: August 2026

Abstract

The extracts of the bio-wastes produce from agricultural wastes and plants have been used for the sustainability, eco-friendly and economic synthesis of different metallic nanoparticles. The present study has proposed synthesizing zinc oxide particles (ZnO) by a green chemistry route using waste tea leaves extract to sequestrate tetracycline antibiotic (TEC) from wastewater. The prepared ZnO NPs were characterized using Scanning Electron Microscope (SEM), X-ray Diffraction (XRD), Fourier Transfrom InfraRed (FTIR), Brunauer–Emmett–Teller (BET) surface area, and through the determination of pH_{pzc}. The surface of the ZnO exhibits a highly heterogeneous texture with irregular, aggregated particles and rough surfaces with a BET surface area of 41.7 m^2/g. Batch adsorption experiments were conducted, and the results showed that the prepared ZnO NPs could effectively adsorb > 95% of TEC from wastewater at the optimal conditions (pH of 5.5, shaking speed 200 rpm, adsorbent dosage 400 mg/100 ml, temperature 298 K, and 100 ppm initial TEC concentration at 120 min contact time). The kinetics of the adsorption describes well by Pseudo-second order model with a K_2 value of 0.004 g/mg-min for a TEC concentration of 100 mg/L, while the mechanism was controlled by external mass transfer and intra-particle diffusion. Langmuir model fitted well the equilibrium adsorption data with a maximum adsorption capacity of 110.56 mg/g, and this provides evidence of a monolayer adsorption phenomenon. Negative ΔH° and ΔG° were indicative of an exothermic and spontaneous nature. Finally, the synthesized ZnO NPs also exhibited good regeneration potential, with only a 31% reduction in efficiency was noticed after five regeneration-adsorption cycles.

Keywords: Adsorption, Tetracycline, Tea leaves, Zinc Oxide nanoparticles, Kinetic, Isotherm

How to Cite: Abd Almajeed, Z. A., Mohammed, A. A. (2026). Efficient Adsorption of Tetracycline from Aqueous Solution onto Zinc Oxide Nanoparticles: Isotherm, Kinetic, Regeneration and Thermodynamic Studies. *Bulletin of Chemical Reaction Engineering & Catalysis*, 21 (2), 385-402. (DOI: 10.9767/bcrec.20555)

Permalink/DOI: https://doi.org/10.9767/bcrec.20555

1. Introduction

The nature of water and the environment is one of the most imperative in modern times. Many factors such as population growth, climate change, pollution, and poor management of water resources, exasperating these problems (1). In recent decades, the increasing pollution levels in the aquatic environment have become a concern for many countries [2]. Drinking water resources are polluted by many elements , whereby heavy metals, dyes, pharmaceuticals and emerging contaminants are among the most groups as they directly affect human health [3]. The pharmaceutical industry is a major source of wastewater effluents containing the aforementioned pollutants [4]. Such pharmaceuticals are widely used because of their effectiveness in treating broad range of illnesses in animals, poultry, fish, and humans [5]. They are also added in small quantities to animal feed as growth promoters [6]. Antibiotics are introduced into aquatic ecosystems through various pathways, such as wastewater effluents,

* Corresponding Author.
Email: zahraa.abd2111m@coeng.uobaghdad.edu.iq (Z.A. Abd Almjeed)

agricultural runoff, and the improper disposal of unused pharmaceuticals [7]. Among these antibiotics, tetracycline is the most commonly used for humane and vetrinary medicine. Many methods have been used to separate antibiotics from wastewater, including but not limited to emulsion liquid membrane [8], electrocoagulation [9], constructed wetlands [10], catalytic ozonation [11], photodegradation [12], biological method [13], fenton-based AOPs [14] and many other methods. However, these treatment processes are often ineffective at completely removing antibiotics, allowing trace concentrations to accumulate in surface and ground water, vary in cost, and their successful implementation depends on local infrastructure and regulatory support [15]. Among the various methods currently employed to remove antibiotics from wastewater is adsorption due to its cost-effectiveness, high efficiency, eco-friendly, ease of practice, and doesn't involve transformation during treatment [16]. Numerous studies using different groups of adsorbent materials have widely highlighted adsorption as a pollutant remediation process in the literature. Material properties such as surface area, functional groups, porosity, and morphology greatly influence the final adsorption capacity [17].

Metal-organic frameworks, biochar, activated carbon, and graphene-based adsorbents have shown high potential for adsorbing antibiotics, require lower expertise and offer shorter treatment time, but it is expensive [15]. Recently, green synthesis of nanomaterials from renewable, abundant, and low-cost materials from waste biomass has been evaluated by many researchers. Green nanotechnology seamlessly incorporates advanced technologies into our everyday routines due to its larger surface area in comparison to bulk materials. This increased surface area enhances their chemical reactivity, as atoms located on the surface exhibit greater activity than those within the core structure. Consequently, green nanotechnology offers a wide range of applications and innovativ solutions [18]. Nanoparticles can be synthesize through biological, chemical or physical approaches. However, chemical and physical synthesis techniques frequently present several limitations, such as the need for special instrument, potential contamination, limited stability, high production costs, and challenges related to re-producability and reliability [19,20]. Moreover, these methods often contain the use of hazardous chemicals, which present considerable risks to both biomedical applications and environmental safety [21]. To reduce the impact of these drawbacks, recently, green synthesis methods of nanoparticles are non-toxic, biodegradable in nature, and cost-effective. Bio-wastes derivable from different parts of natural plants, such as fruit peels, bark, and flowers, are rich in essential phytochemicals including tannins, phenolics, alkaloids, and terpenoids. These plant-based wastes are readily present in the environment, make them a valuable and sustainable resources [22].

These phytochemicals function as both reducing and stabilizing agents in the formulation of metal oxide from their corresponding precursor solutions. Green nanotechnology offers innovative approaches for wastewater treatment and of toxic contaminants removal, so, supporting the realization of sustainable development goals accompanying the provision of clean drinking water. [23]. Of the various metal oxides, ZnO nanoparticles exhibit large excitation binding energy, high electron mobility, optical transmittance, and high electron mobility [19]. Recently, many studies have synthesized ZnO nanoparticles using plant extracts from different plants [20].The limitations include potential challenges in scaling up the synthesis of ZnO nanoparticles. Tea leaves are cheap, include a range of chemical compounds like tannins, catechins, volatile oils and caffeine, each with its own solubility characteristics. Catechins are polyphenolic compounds possess various levels of solubility in different solvents based on different factors like temperature, pH and polarity. These catechins play different roles in shaping the flavor profile and health benefits of tea leaves. Notably, the total content of catechins in green tea can account for up to 30% of the dry weight of the tea leaves Furthermore, some other plants also contain catechins, but in lesser quantities than tea [24;25] and can also be used for the green preparation of ZnO NPs. To the best of our knowledge no previous work on the removal of tetracycline from wastewater by adsorption using zinc oxide prepared from tea leaves. Hence, as a novelty and in view to full in the paucity of published data on the use of biomass based adsorbent for removing TEC, the adsorption of TEC was investigated by using green zinc oxide nanoparticles to give some cues for future research and applications contributing to the improvement of efficiency of the adsorption process by promoting circular economy practices and minimizing organic waste . The present work focuses on: (1) the green producing of zinc oxide nanoparticles using waste tea leaves extracts and testing the ability to adsorbed tetracycline, (2) investigating the physiochemical characteristics of the zinc oxide nanoparticles via FTIR, XRD, SEM, BET and TEM, (3) evaluating the TEC removal efficiency under various experimental conditions, (4) studying the thermodynamic, isotherm and kinetic of adsorption process and (5) investigate the desorption of tetracycline and the regeneration of ZnO nanoparticles.

2. Materials and Method

2.1. Materials

Tetracycline hydrochloride ($C_{22}H_{24}N_2O_8$) in powdered form was sourced from a certified pharmaceutical manufacturer in Iraq, and utilized as received without further purification. Physicochemical properties of tetracycline are molecular weight 480.9 g/mol and Purity 98 %,. One gram of TEC was dissolved in 1L deionized water under vigorous agitation for 25 min to prepare a homogeneous 1000 mg/L stock solution.

2.2. ZnO Synthesis

Before starting the experiments, all glassware was autoclaved to remove any contamination. Initially, 10 g of tea leaves are subjected to washing to remove dust particles, drying, and converted to small pieces before being boiled in 100 mL of distilled water at 80 ˚C for 2 h to prepare their extract. Then, 100 mL aqueous tea extract was transferred to a 500 mL beaker and positioned above a magnetic stirrer (hot plate with magnetic stirrer). The rotation per minute (rpm) and temperature were set at 4000 rpm and 80˚C, respectively. Then, 0.01 M solution of ($Zn(NO_3)_2 \cdot 6H_2O$) as the inorganic metal oxide was prepared in distilled water and 250 mK of this solution was gradually added. After the addition of zinc nitrate, the pH was adjusted to 11 and magnetically stirred until the reaction mixture turned pale yellow. Then the mixture was naturally left to cool to 25 ˚C. The resulting precipitate was allowed to settle before being separated from the mixture via centrifugation at 4000 rpm for 10 min. The resulting solid was then washed with deionized water to eliminate residual impurities, followed by drying in an oven at 60 °C. After that, the ZnO nanoparticles were grashed and stored in a sealed, airtight container.

2.3. Characterizations

Transmission electron microscopy (TEM) was employed to determine the nanostructure of ZnO nanoparticles. FTIR spectra were used for the functional groups examination on the ZnO surfaces in the range of 350 - 4000 cm^{-1}. The structure and the morphology of the prepared ZnO NP were examined using scanning electron microscopy (SEM). The pore size distributions and specific surface area were examined by Brunauer-Emmett-Teller (BET) analysis (Quantachrome Nova1000 e, Germany). Finally, the crystallinity and structure of the prepared sample were examined using X-ray diffraction (XRD) Patterns, the measurements were carried out on a Siemens D-500 diffractometer operated at 40 mA and 40 kV, using Cu-Kα radiation (λ = 1.5418 Å), with a scan rate of 0.05˚ S^{-1} over a 2θ range of 0–80˚. These characterization techniques provided complementary insights into the structural order, surface chemistry, and elemental distribution of the synthesized material, enabling a deeper understanding of its potential performance in the intended application.

2.4. Batch Experiments

The effect of various parameters on TEC sequestration percent by ZnO such as initial pH (3–9), ZnO dosage (0.1–0.5 g per 100 mL of TEC solution), contact time (up to 120 min , 150–250 rpm agitation speed, initial TEC concentration (25–150 mg/L) and temperature (25 – 45 ˚C) was investigated. A stock solution of 1000 mg/L prepared and kept at 30 ˚C. This solution was further diluted to obtain the required TEC concentrations. Kinetic adsorption experiments were conducted at 298 K using an initial pH value of 5.5, which was adjusted using 0.1 M NaOH and 0.1 M HCl. For each experiment, 100 ml of TEC solution was added to 0.4 g of ZnO. After adsorption, the mixture was filtered using 0.45 µm filter paper to separate ZnO, and the residual TEC concentration was quantified using a UV–Vis spectrophotometer at the maximum absorbance wavelength of 200 nm.
Equations (1) and (2) were subsequently employed to calculate the removal efficiency (percent) and uptake (qe) of the adsorbent, respectively [26].

$$\text{Removal Efficiency (\%)} = \frac{C_0 - C_e}{C_0} \times 100 \quad (1)$$

$$q_e = \frac{(C_0 - C_e)V}{m} \quad (2)$$

Where, C_0 and C_e represent the initial and final TEC concentrations (mg/L) respectively, V presents volume of the TEC solution (L), m denotes the adsorbent mass (g) and q_e (mg/g) is the quantity of TEC adsorbed onto zinc oxide.

2.5. The Zero Charge Point (pHpzc)

To ascertain the zero charge point of Zinc oxide adsorbent, 40 mL (0.1 M KNO_3 was prepared. Then the pH of the prepared solution (2 -12) was then attuned by the addition of 0.1 M NaOH and/ or HCl. Then, shaken for 24 hours at 150 rpm under 30 °C with the add-on a specific volume of zinc oxide particles. After filtering the pH was measured. The point zero charge of the adsorbent was get by plotting the (initial -final) pH vs. the final pH (4).

3. Results and Discussion

3.1. Adsorbent Characterizations

The X-ray diffraction (XRD) represents one of the most important methods of material crystallinity investigation (27). The XRD pattern of the synthesized sample, presented in Figure 1, confirms the successful formation of crystalline zinc oxide. The diffraction peaks are intense and

sharp, indicating a high degree of crystallinity. The most outstanding diffraction peaks are ascertained at 2θ values of approximately 31.7°, 34.4°, 36.2°, 47.5°, 56.6°, 62.8°, 66.4°, 67.9°, and 69.1°, which match to the (100), (002), (101), (102), (103), (110), (200), (112), and (201) crystallographic planes, respectively, these reflections are in excellent agreement with the standard hexagonal wurtzite structure of ZnO, as indexed by (JCPDS card No. 36-1451) [28]. The distinct diffraction peaks observed match various crystal planes characteristic of hydrotalcite-like materials, while the narrow peaks are attributed to the great crystallinity of the synthesized particles [29,30]. The absence of any secondary phases or impurity peaks indicates the high purity of the synthesized nanoparticles. Furthermore, the intensity and sharpness of the diffraction peaks indicate a high degree of crystallinity. Based on the full width at half maximum of the most intense peak (usually related to the (101) plane at 36.20°), the average crystallite size can be estimated using the Scherrer equation. These findings are in good accordance with earlier reports on ZnO nanostructures [31].

The FTIR spectrum of the prepared ZnO displayed in Figure 2, provides insight into the surface functional groups and chemical bonds present within the sample. The absorption peak observed at 3425.58 cm^{-1} is ascribable the stretching vibrations of hydroxyl (–OH) functional groups, which maybe originate from adsorbed water molecules or surface-bound hydroxyl groups. This is further supported by the weak bending vibration at 1631.78 cm^{-1}, typically associated with H–O–H bending of physisorbed water. The distinct absorption at 1762.94 cm^{-1} may be attributed to C=O stretching vibrations of

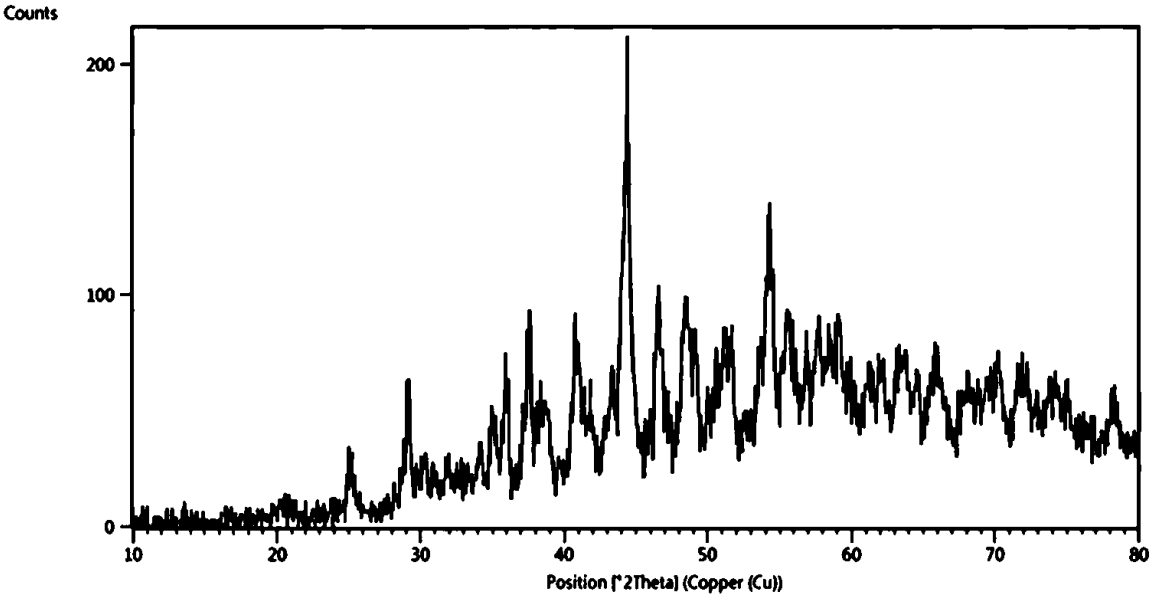

Figure 1. (A) SEM image, (B) SEM-EDX mapping, followed by its materials constituent, (C) Tungsten (W), (D) Bi (Bismuth), (E) Mo (Molybdenum), and (F) their ternary diagram in W-based POM composite.

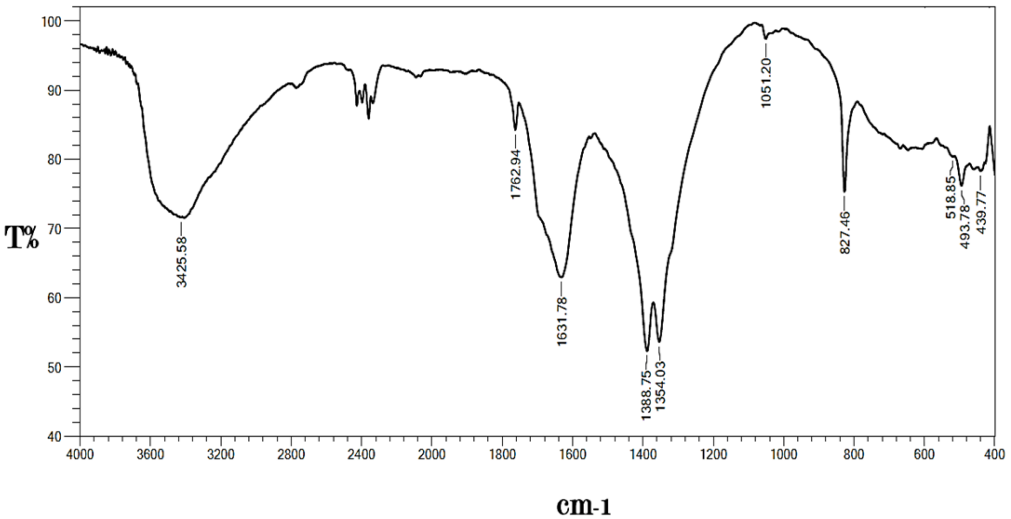

Figure 2. FTIR characterization of ZnO.

surface-bound carboxylic or carbonyl groups, possibly originating from residual organic precursors or atmospheric CO_2 adsorption during synthesis. Additionally, the band ascertained at 1388.75 cm^{-1} can be linked to symmetric stretching vibrations of carbonate (CO_3^{2-}) species, while the peak at 1354.03 cm^{-1} may also be associated with C–O stretching modes. The sharp and well-defined band at 1051.20 cm^{-1} might indicate the presence of residual nitrate or sulfate groups, often retained from precursor salts used in wet chemical or sol-gel synthesis methods. The weak band at 827.46 cm^{-1} could correspond to out-of-plane bending vibrations of O–H groups or contributions from M–OH bonds. Most importantly, the series of absorption bands in the range of 400–600 cm^{-1}, specifically at 518.85 cm^{-1}, 493.38 cm^{-1}, and 439.77 cm^{-1}, are indicative of Zn–O stretching vibrations associated with crystal structure of ZnO. These bands confirm the successful formation of ZnO and reflect the metal–oxygen framework within the lattice [32, 33]. The FTIR analysis supports the XRD findings by confirming the existence of Zn–O bonds indicative of ZnO formation. Additionally, the existence of –OH, C=O, and CO_3 groups suggests surface-bound species or minor residuals from the synthesis process, which may play a role in surface reactivity and interaction with adsorbates in applications such as adsorption.

The morphology of the adsorbent's surface before and after the adsorption was investigated using SEM analysis. Figure 3A-B illustrates the surface morphology of ZnO before and after adsorption. As observed in Figure 3A, the surface of the ZnO exhibits a highly heterogeneous texture with aggregated, irregular particles and rough surfaces, indicative of a porous structure capable of providing multiple active adsorption sites. The existence of plate-like and flaky structures suggests the layered nature matrix , which assist enhanced surface interaction with the target contaminant. The surface appears smoother and more compact, with a decrease in the visible porosity and a more uniform particle distribution. This morphological changes means the successful occupation of active sites by the TEC molecules and possible partial pore blockage, confirming the capacity of adsorbent. These results provide indication of the structural compatibility and high adsorption potential of ZnO forTEC sequstration, agrees with previous studies [34], and reinforce the efficiency of this material in real-world applications

The pore structure properties of ZnO, as determined by BET analysis, indicate a BET surface area of 41.7 m^2/g, a pore volume of 0.091 cm^3/g, and an average pore diameter of 14.7 nm. According to these measurements, the synthesized ZnO falls within the nanoscale range, as the average pore diameter is less than 100 nm, in agreement with the criteria reported in previous studies for classifying materials as nanostructured.

TEM analysis was employed to elucidate the internal morphological structure of the synthesized nanomaterial and to acquire crucial data concerning the dimensions, composition, structure, and other characteristics of the nanoadsorbent. As depicted in the TEM micrographs (Figure 4), the ZnO exhibits an irregular morphology. However, the majority of

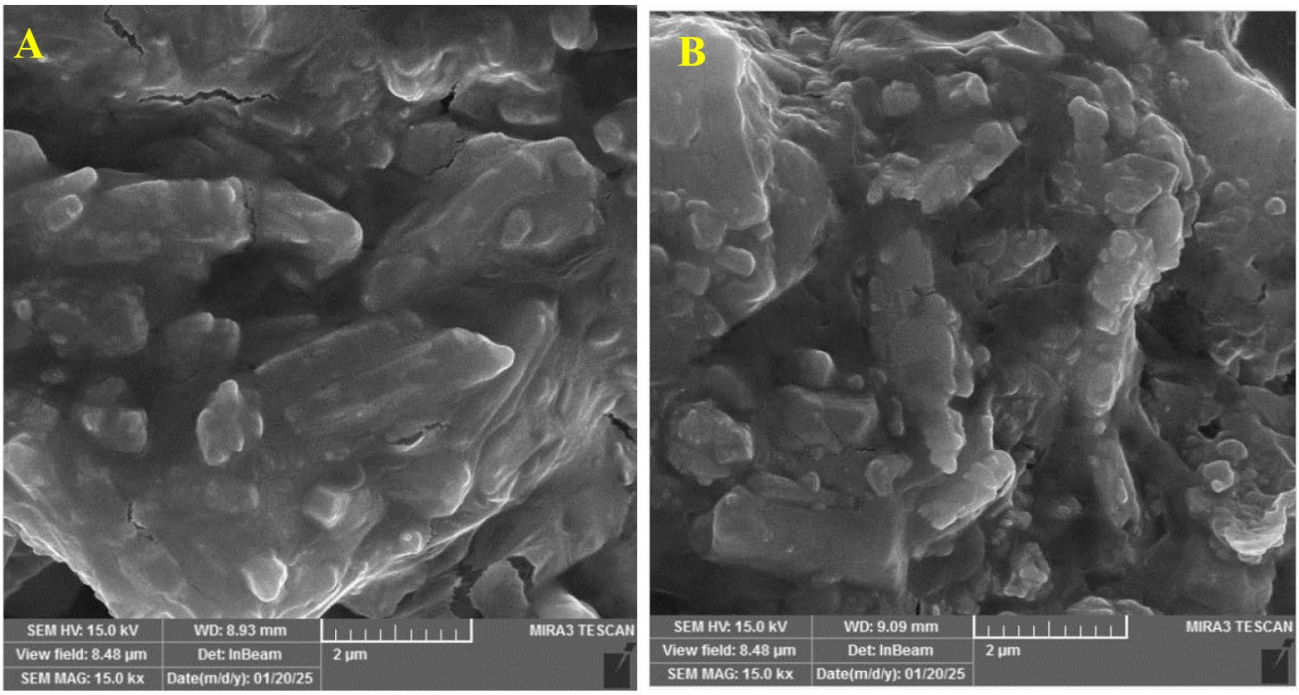

Figure 3. SEM images (A) ZnO before adsorption, and (B) ZnO after adsorption.

the particles are typically integrated hierarchical structures comprising crystallites of varying sizes, ranging from spherical to rod-shaped. Its distribution was optimized to provide an adequate number of active sites without becoming so dense as to cause site blockage.

3.2. Affecting Parameters on TEC Adsorption

The pH of the solution is a critical parameter that significantly influences the surface charge of the adsorbent and the ionization state of the pollutant, thereby controlling speciation in solution, and the overall adsorption mechanism [35]. Contact time is another key factor, as prolonged interaction between adsorbent and adsorbate generally increases removal percent until equilibrium is attained [16]. In the present study, the removal percent was investigated over a pH range (3–9) and different contact time (5–180 min). As shown in Figure 5, removal percent enhanced with increasing contact time at all pH values, reaching near-equilibrium between 120 and 180 min. The maximum removal of (84%) was obtained at pH of 5.5, suggesting that this pH provides an optimal balance between adsorbent surface charge and the ionic state of tetracycline, thus maximizing electrostatic attraction and availability of active sites. At strongly acidic conditions (pH of 3), the removal efficiency remained low, even at extended contact times, likely due to excessive protonation of both ZnO surface and tetracycline molecules, resulting in competition with H^+ ions for adsorption sites. At pH of 7, a slight decrease was observed compared with the optimum, which can be attributed to the surface approaching neutrality or becoming slightly negatively charged, thereby reducing attractive interactions. The newly tested alkaline conditions, pH of 8 and 9, showed a more pronounced decline in removal efficiency relative to the acidic-to-neutral region. This decrease can be explained by the point of zero charge of ZnO (pH_{pzc} = 7.5, Figure 5A). Above this value, the ZnO surface acquires a negative charge, while tetracycline species are predominantly anionic. Consequently, electrostatic repulsion between the adsorbent surface and tetracycline reduces adsorption efficiency. Additionally, competition from OH^- ions for surface sites and changes in tetracycline speciation may further hinder adsorption under alkaline conditions. Overall, these results confirm that adsorption is highly pH-dependent, with pH of 5.5 and a contact time of 120 min providing the most favorable conditions. This behavior aligns with the surface chemistry of ZnO and the speciation of tetracycline, reinforcing the combined importance of solution pH and interaction time in optimizing adsorption performance.

The adsorbent dosage is an additional parameter that has a direct effect on the sequestration of TEC from solution [36]. The combined influence of contact time and ZnO dosage on TEC removal efficiency is illustrated in Figure 6. The study investigated adsorbent dosages in the range (0.1 - 0.5 g/100 mL) in contact with a 50 mg/L TEC solution, under constant pH of 6 and agitation speed of 200 rpm at interaction time for up to 120 minutes. As ascertained in the Figure 6, the removal percent increased progressively with extended interaction time for all tested dosages. This behavior indicates that TEC uptake onto the ZnO composite is time-dependent, especially during the initial stages (first 60 minutes), where a rapid rise in removal efficiency is noted. This is likely due to the abundant availability of active sorption sites on the adsorbent surface, enabling fast external surface adsorption and intraparticle diffusion. At each time point, increasing the adsorbent dosage enhanced the removal efficiency up to a certain threshold. Specifically, 0.4 g/100 mL adsorbent dosage yielded the highest TEC removal (~91%) after 120 minutes, indicating that this dosage offers an optimal balance between surface area availability and contaminant load. The improvement in removal with higher dosage is

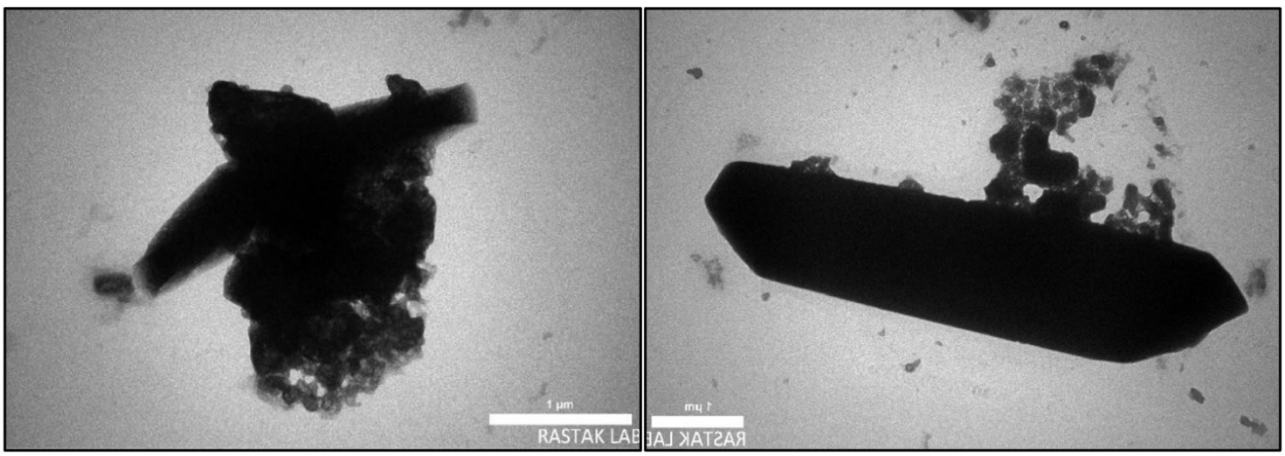

Figure 4. TEM images of the ZnO adsorbent.

primarily attributed to enhance the surface area, which increase the binding sites on the surface which enhance adsorbate–adsorbent interactions allowing more TEC to be adsorbed [37]. However, further increase in the dosage to 0.5 g/100 mL resulted in a slight decline in removal efficiency (~84%). This phenomenon is attributed to possible interference between the binding sites due to the increased of adsorbent dosage which leads to reduced effective surface area and pore blockage. Such effects limit the accessibility of binding sites for TEC molecules and may introduce mass transfer resistance due to a decreased inter-particle distance and stronger adsorbate-adsorbate repulsion on closely packed surfaces. These findings align with commonly observed behavior in solid-liquid adsorption systems, where an optimal adsorbent dosage exists beyond which efficiency either plateaus or decreases due to physicochemical constraints. So that, 0.4 g/100 mL was selected as the optimal dosage for the next experiments, as it offered the highest removal efficiency while maintaining material economy and adsorption site availability.

To evaluate the influence of agitation speed on the external mass transfer process, three different speeds were investigated at the best pH and adsorbent dosage using ZnO. As represented in Figure 7, the removal percent enhanced with increasing contact time for all agitation speeds, reflecting the time-dependent nature of the adsorption process. Notably, the system at 200 rpm achieved the highest removal efficiency along all intervals, achieving approximately 90% at 120 minutes contact time in comparison to 84% and 86% at 150 and 250 rpm, respectively. At lower

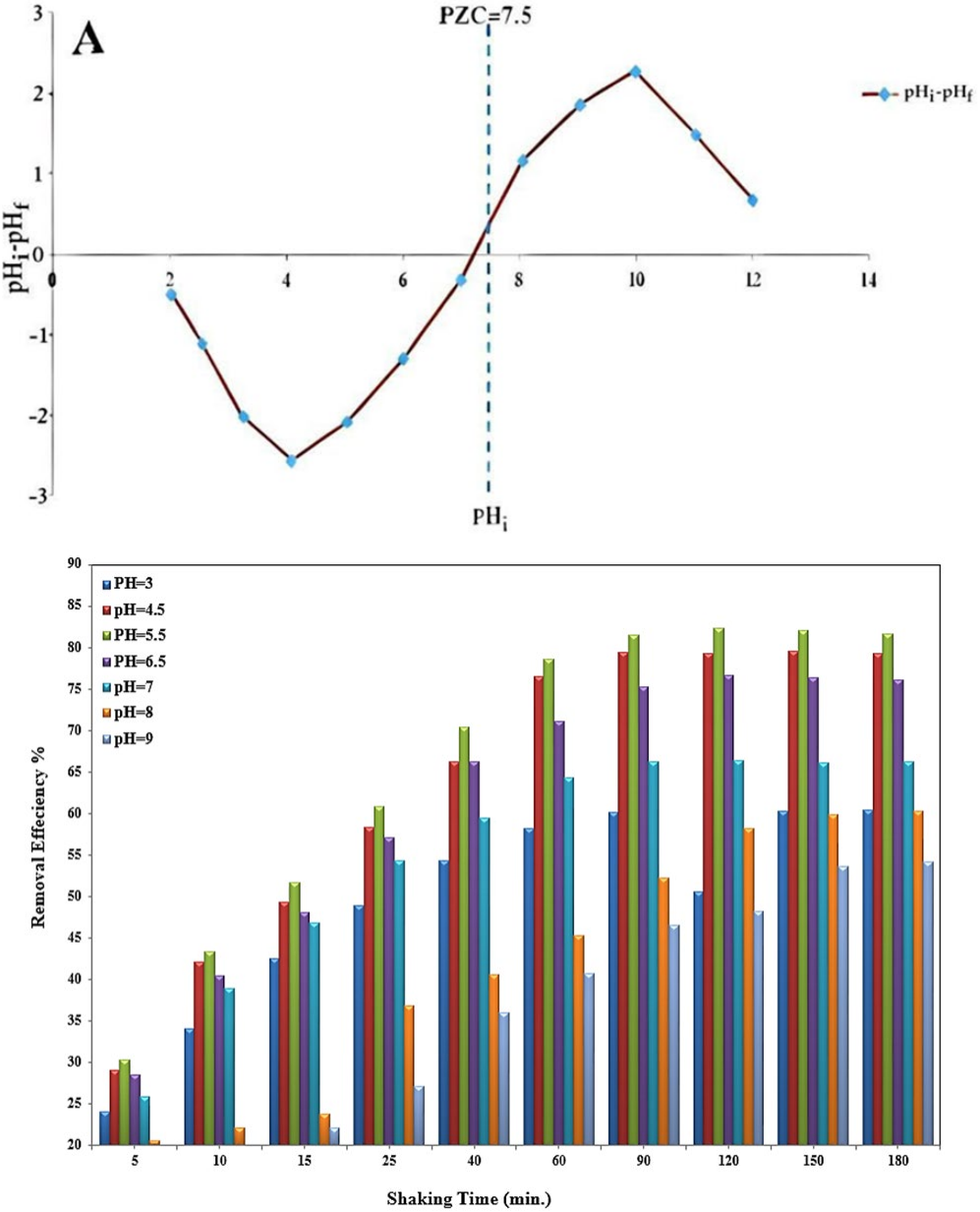

Figure 5. (A) pH_{PZC} for ZnO, (B) The influence of pH on TEC removal onto ZnO at (TEC Conc. = 50 mg/L, T = 30 °C, Shaking Speed = 200 rpm, Dosage of adsorbent = 0.2 g/100 mL, and Time = 180 min.).

agitation (150 rpm), limited dispersion of adsorbent particles likely hindered access to active binding sites, reducing removal. While higher agitation (250 rpm) initially improved mixing, excessive turbulence may have disrupted equilibrium by causing particle aggregation or desorption. These findings suggest that moderate agitation (200 rpm) offers the most favorable conditions for efficient TEC removal, and it was thus adopted in subsequent experiments.

The influence of both the initial TEC concentration and the interaction time on the adsorption capacity and removal efficiency was investigated at pH of 6, using 0.4 g/100 mL ZnO dosage and 200 rpm agitation speed. The results are shown in Figure 8(A-B), which reveal the relationship between different initial concentrations (25–150 ppm) and contact time (5–120 min). As seen in Figure 8A, the removal percent increases with prolonged shaking time for all concentrations. A rapid increase is observed within the initial 30–40 minutes, then a slower rate of increase until equilibrium is approached at around 90–120 minutes. At each time point, the removal efficiency is inversely proportional to the initial concentration, at 120 minutes, reaches approximately 95% removal efficiency for 100 ppm initial TEC concentration, while it remains lower (~81%) for 150 ppm. This behavior may be attributed to the saturation of available active sites on the adsorbent surface, where the adsorption capacity is related to the active site of the adsorbent meaning that the adsorption of the adsorbate stops when all sites on the adsorbent surface have interacted with the adsorbate [38]. At lower initial concentrations, the ratio of available adsorption sites to contaminant molecules is higher, allowing for more effective removal. In contrast, at higher concentrations, the relative scarcity of active sites results in a decrease in removal percentage due to overcrowding and site saturation. In a Figure 8B shows that the uptake (mg/g) increases with both contact time and initial concentration. This is

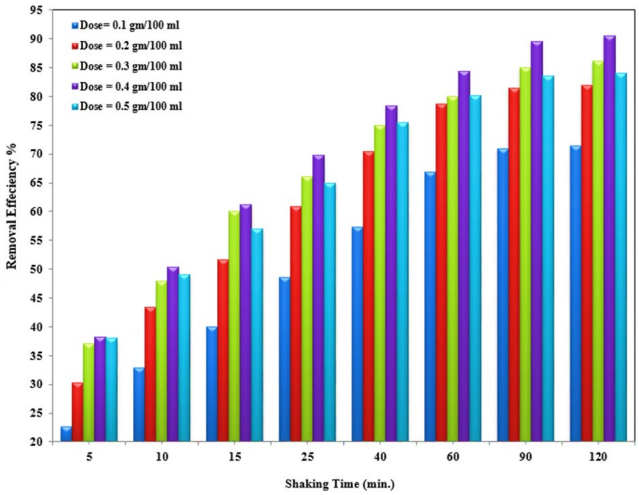

Figure 6. The influence of the ZnO dosage on the sorption at (Conc. of adsorbate = 50 mg/L, T = 30 °C, Shaking Speed = 200 rpm, pH = 5.5).

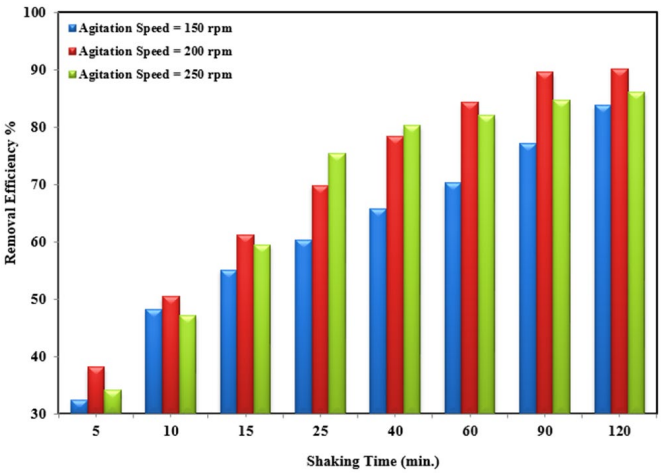

Figure 7. The influence of agitation speed on sorption onto ZnO at (Conc. of adsorbate = 50 mg/L, T = 30 °C, Dosage of adsorbent = 0.4 g/100 mL, pH=5.5).

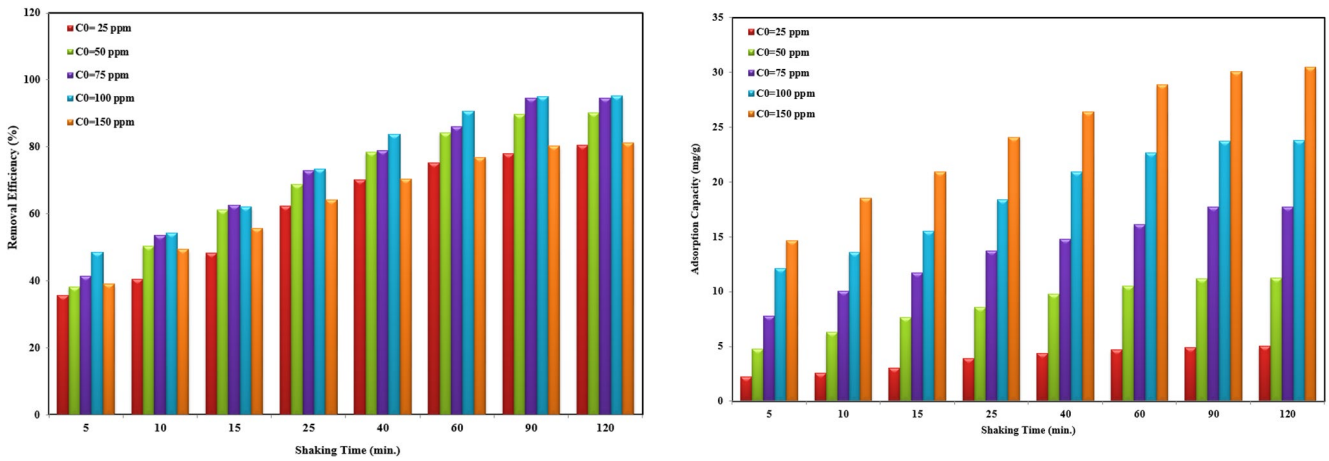

Figure 8. The effect of (A) initial concentration, and (B) adsorption uptake on the TEC sorption onto ZnO at (T = 30 °C, 200 rpm, Dosage of adsorbent = 0.4 g/100 mL, pH = 5.5).

consistent with expectations, as a higher concentration creates a stronger concentration gradient, which acts as the driving force for mass transfer between the aqueous phase and the adsorbent. As the initial concentration increases from 25 to 150 ppm, the adsorption capacity rises markedly, with the maximum capacity exceeding 30 mg/g at 150 ppm after 120 minutes. This indicates that the adsorption process is more efficient at higher concentrations. At lower concentrations, monolayer adsorption dominate, while multilayer adsorption becomes more likely at higher concentrations, due to the availability of additional contaminant TEC molecules and interactions between molecules and adsorbed species [39]. The initial fast adsorption phase is due to the availability of a larger number of active sites, which allows for easy access and strong interaction with the target molecules. As time progresses, these sites become increasingly occupied, and the process slows down due to steric hindrance and repulsive forces among adsorbed molecules [40]. Beyond 90 minutes, the system reaches near-equilibrium, indicating that most available binding sites are saturated and no further significant uptake occurs. Similar behavior on the effect of the adsorbate concentration on the removal efficiency has been reached by researcher [41] for the adsorption of methylene blue from the aqueous phase onto rice husk ash.

3.3. Adsorption Thermodynamics and Temperature Effects

Temperature is a further vital parameter for the sorption process. The effects of four different temperatures on the adsorption of TEC onto zinc oxide particles are investigated and the results presented in Figure 9 (A and B) reveal a decline in adsorption efficiency from 94% to 82.5% as the temperature increased from 298 K to 318 K. This decrease suggests that higher temperatures reduce adsorption effectiveness, likely due to enhanced mobility of adsorbate molecules, which promotes desorption over adsorption. As the temperature rises, the adsorbate tends to overcome the attractive forces of the adsorbent, leading to the deactivation of active sites on the surface and thus a decrease in performance.

Table 1. Thermodynamic parameters.

Temperature (K)	ΔG° (J/mol)	ΔS° (J/mol. K)	ΔH° (J/mol)
298	-3381	-235	-68500
303	-2093		
308	-1551		
318	-0343		

According to these results the adsorption process is exothermic reaction. This behavior is in agreement with the findings of [42], who reported similar thermal sensitivity in adsorbent systems. From a thermodynamic perspective, entropy change (ΔS°) is considered a key driving force for adsorption in isolated systems [43]. Thermodynamic parameters including enthalpy change (ΔH°), entropy change (ΔS°), and Gibbs free energy change (ΔG°) were calculated using the Van't Hoff equation [44]:

$$K_2 = \frac{q_e}{C_e} \quad (3)$$

$$\Delta G^\circ \text{ (kJ/mol)} = - R\ T \ln K_2 \quad (4)$$

$$\ln K_2 = \frac{\Delta S^\circ}{R} - \frac{\Delta H^\circ}{RT} \quad (5)$$

where, T (K) and R (8.314 J/mol.K) represents the temperature and the constant of universal gas, respectively.

The thermodynamic parameters (ΔH°, ΔS°, and ΔG°) derived from the Van't Hoff plot are presented in Table 1. The negative value of ΔS° suggests a decrease in randomness at the solid–liquid interface during the adsorption of tetracycline (TEC) onto ZnO, indicating a more ordered interfacial structure. The exothermic nature of the process is confirmed by the negative ΔH°, while the negative ΔG° values across the studied temperatures confirm the spontaneity and thermodynamic favorability of the adsorption process.

3.4. Reusability of ZnO and Desorption of TEC

A series of five sequential adsorption–desorption experiments was done. For the desorption phase, 0.4 g of previously used ZnO was treated with 0.2 M hydrochloric acid, stirred continuously for 2 hours, then subjected to filtration, rinsing, and drying before reuse. TEC removal efficiency was monitored across the cycles using Equation (2). As shown in Figure 10, a noticeable reduction in efficiency occurred over time, with the value declining to 61% by the fifth cycle. This decrease is likely due to the progressive deactivation of adsorption sites, possibly caused by physicochemical modifications to the ZnO surface during repeated regeneration steps. As a result, zinc oxide particles work well to adsorb tetracycline from aqueous solution. The comparison of the uptake of the present study with other previous studies is depicted in Table 2. These results indicated that ZnO adsorbent is a relatively efficient adsorbent for the sequestration of tetracycline antibiotic from the liquid phase.

3.5. Adsorption and Desorption Kinetics

3.5.1. Adsorption kinetics

The effectiveness of a sorption system is primarily influenced by the rate at which

contaminants migrate from the aqueous phase to the surface of the adsorbent. The adsorption rate serves as a key parameter for interpreting the adsorption process. Adsorption kinetics not only determine the rate of molecule uptake but also provide insight into the required residence time in both batch and continuous systems, as well as the overall performance of the adsorbent [57]. To analyze the experimental kinetic data, the following kinetic models were applied.

Pseudo-first-order (PFO) model as in Equation (6) describes the rate at which the sorbate is adsorbed from the aqueous solution onto the adsorbent surface [58]:

$$\ln(q_e - q_t) = \ln q_e - K_1. \quad (6)$$

where, q_e and q_t (mg/g) denote the amounts of contaminant adsorbed onto the solid adsorbent at equilibrium and at a given time t, respectively, while K_1 (min^{-1}) represents the pseudo-first-order rate constant.

The Pseudo-Second-Order (PSO) model as represented in Equation (7), assumes that the adsorption process involves the formation of a monolayer of the contaminant on the adsorbent surface. It further presumes the absence of interactions among adsorbed species and a uniform sorption energy across all active sites of the adsorbent [34].

$$\frac{t}{q_t} = \frac{t}{q_e} + \frac{1}{q_e^2 . K_2} \quad (7)$$

Table 2. Maximum adsorption capacity (q_{max}) of TEC using different adsorbents.

Adsorbent	Temp. (K)	Dosage (mg/L)	pH	Initial conc. (mg/l)	Shaking speed (rpm)	Time (h)	q_{max} (mg/g)	Ref.
Fe_3O_4@SiO_2-chitosan/graphene oxide	298	500	7	100	80	1	110.22	[45]
α-Fe_2O_3/RGO	298	80	6	10	180	1.5	9.690	[46]
Cu-immobilized alginate beads	.15318	1000	3	90	150	3	58.57	[47]
Pistachio shell powder @ zinc oxide	298	1000	5	60	150	2	98.717	[48]
ZnO/Fe_3O_4 Magnetic Nanocomposite	298	500	7.5	50	150	2	80.1	[49]
Cerium oxide nanoparticles	313	600	6	125	150	1	57.14	[50]
Vitamin B6 @ biochar	298	1000	7	60	150	2	76.92	[51]
Zero-valent Iron @ AC	298	1000	7.1	50	150	1	81.5	[52]
AC @ zeolitic imidazolate	298	1000	7	50	250	2	35.64	[53]
$CuCoFe_2O_4$ @ Chitosan	298	400	3.5	5	150	0.333	4.484	[54]
Alkali acid-modified magnetic biochar	298	500	10	50	150	24	97.96	[55]
Geopolymers from tourmaline tailings (TMT-GP1.2)	318	500	5	10	150	5	105.4	[56]
CaMgAl-LDH/RM	298	400	6	70	150	1.5	108.753	[4]
ZnO	298	400	5.5	100	200	2	110.56	Current study

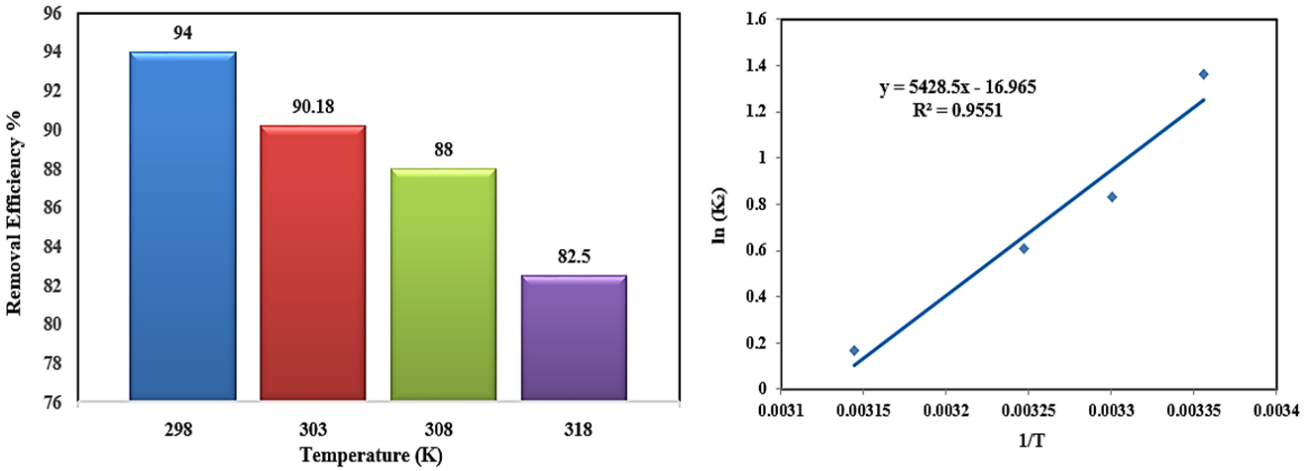

Figure 9. The temperature effect on the adsorption of TEC.

where, K_2 (g/mg.min) denotes the pseudo-second-order (PSO) rate constant.

At the initial stage of adsorption ($t \rightarrow 0$), this model is employed to determine the initial adsorption rate h (mg/g·min), as calculated using Equation (8):

$$h = K_2 . qe^2 \quad (8)$$

Intraparticle Diffusion Model (IPD): this model, introduced by Weber and Morris, is expressed through Equation (9):

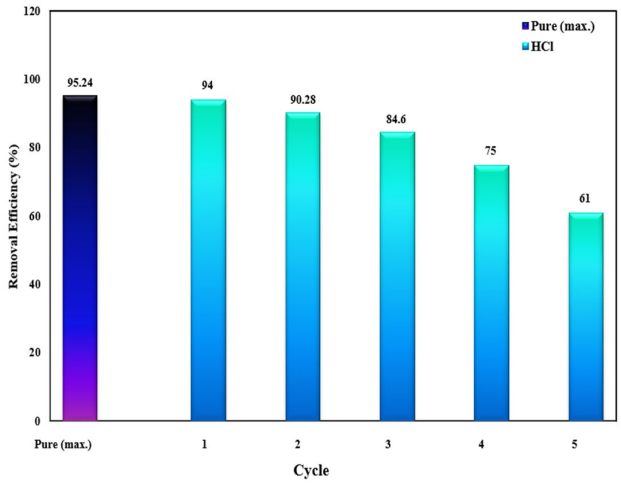

Figure 10. The reusability of ZnO and TEC desorption.

$$q_t = k_i . t^{1/2} + C \quad (9)$$

where, K_i and C represent rate constant (mg/g. $min^{1/2}$) and intercept value, respectively.

The adsorption behavior of TEC onto the ZnO composite was investigated as a function of time under varying initial contaminant concentrations, and the experimental data were interpreted using different kinetic models. The kinetic parameters and corresponding determination coefficients (R^2) are summarized in Table 3. Among the applied models, the PSO model exhibited a higher R^2 value compared to the PFO model, and its calculated adsorption capacity closely matched the experimental value. Also, these results confirms that parts of the TEC adsorption process on the ZnO surface are controlled by the chemisorption as the rate-limiting step. (Figure 11 A and B).

To determine the intra-particle diffusion (IPD) constants (Equation 9), a linear regression fitting approach was employed, with the results presented in Table 3. The IPD plots (Figure 11 C) display multilinear trends, implying that the TEC adsorption process involves multiple sequential mechanisms. In the initial stage ("portion 1"), a sharp slope is observed, suggesting rapid external surface adsorption facilitated by the abundance of available active sites. This phase typically occurs within the first two minutes. In the subsequent

Table 3. Kinetic parameters of TEC adsorption onto ZnO particles.

Kinetic Model	Parameter	C_0 (mg/L)				
		25	50	75	100	150
Pseudo-first-order	$q_{exp.}$(mg/g)	5.03	11.27	17.74	23.81	30.49
	q_e (mg/g)	3.16	7.73	20.67	20.30	19.07
	K_1 (min^{-1})	0.0356	0.0722	0.066	0.24	0.0419
	R^2	0.985	0.9653	0.8572	0.6608	0.9962
Pseudo-second-order	q_e (mg/g)	5.44	12.17	19.12	25.58	32.47
	K_2 (g/mg) min	0.01838	0.00908	0.00557	0.00470	0.00396
	R^2	0.9988	0.9995	0.9985	0.9987	0.9994
	h (mg/g) min	0.54	1.34	2.04	3.07	4.18
Intra particle-diffusion	$K_{int\ 1}$ (L/mg) $min^{1/2}$)	2.1359	3.4798	5.4305	0.9937	6.5454
	C_1 (mg/g)	0	0	0	0	0
	R^2_1	1	1	1	1	1
	$K_{int\ 2}$ (L/mg) $min^{1/2}$)	1.2084	1.7276	2.2318	0.5655	2.8468
	C_2 (mg/g)	0.9661	0.9587	0.994	0.9791	0.9701
	R^2_2	0.9661	0.9587	0.994	0.9791	0.9701
	$K_{int\ 3}$ (L/mg) $min^{1/2}$)	0.442	0.9198	0.8787	0.1549	1.1545
	C_3 (mg/g)	7.0432	8.9972	15.553	3.436	19.371
	R^2_3	0.9924	1	0.964	0.9553	0.9394

phase ("portion 2"), the slope becomes less steep, indicating a transition to intra-particle diffusion as the rate-controlling step. Finally, in the equilibrium phase ("portion 3"), the slope plateaus, reflecting diffusion limitations due to the lower concentration of residual TEC in solution.

Furthermore, the Arrhenius equation was employed to evaluate the activation energy (E_a) of the adsorption process, providing insight into the energy barrier associated with TEC uptake onto ZnO. To determine the activation energy (E_a) according to adsorption kinetics, the value of h is calculated using Equation (10):

$$h = (1/b) \quad (10)$$

Then the activation energy (E_a) can be calculated using Equation (11):

$$E_a = R\,T\,(\ln h - \ln k) \quad (11)$$

where, k is the rate constant of the second order reaction and b is the coefficient of the second order kinetics equation. According to Equation 11, the activation energy of TEC adsorption process onto zinc oxide is found equal to 15.130 kJ/mole.K.

3.5.2. Kinetics of desorption

Desorption kinetics were analyzed using PFO and PSO models to evaluate the recovery rate [59]. In this study, the kinetic behavior of the experimental desorption data was interpreted using Figure 12. The modified PFO model assumes that the rate of desorption is directly proportional to the number of adsorption sites occupied by tetracycline (TEC), as represented in Equation (12):

$$\frac{dq}{dt} = -K_{1,\mathrm{des}}.\,q \quad (12)$$

where, $K_{1,\mathrm{des}}$ denotes the 1st order rate constant (min^{-1}). The modified PSO model scribe the desorption rate as being the square of the number of fill sites (Equation (13)):

$$\frac{dq}{dt} = -K_{2,\mathrm{des}}.\,q^2 \quad (13)$$

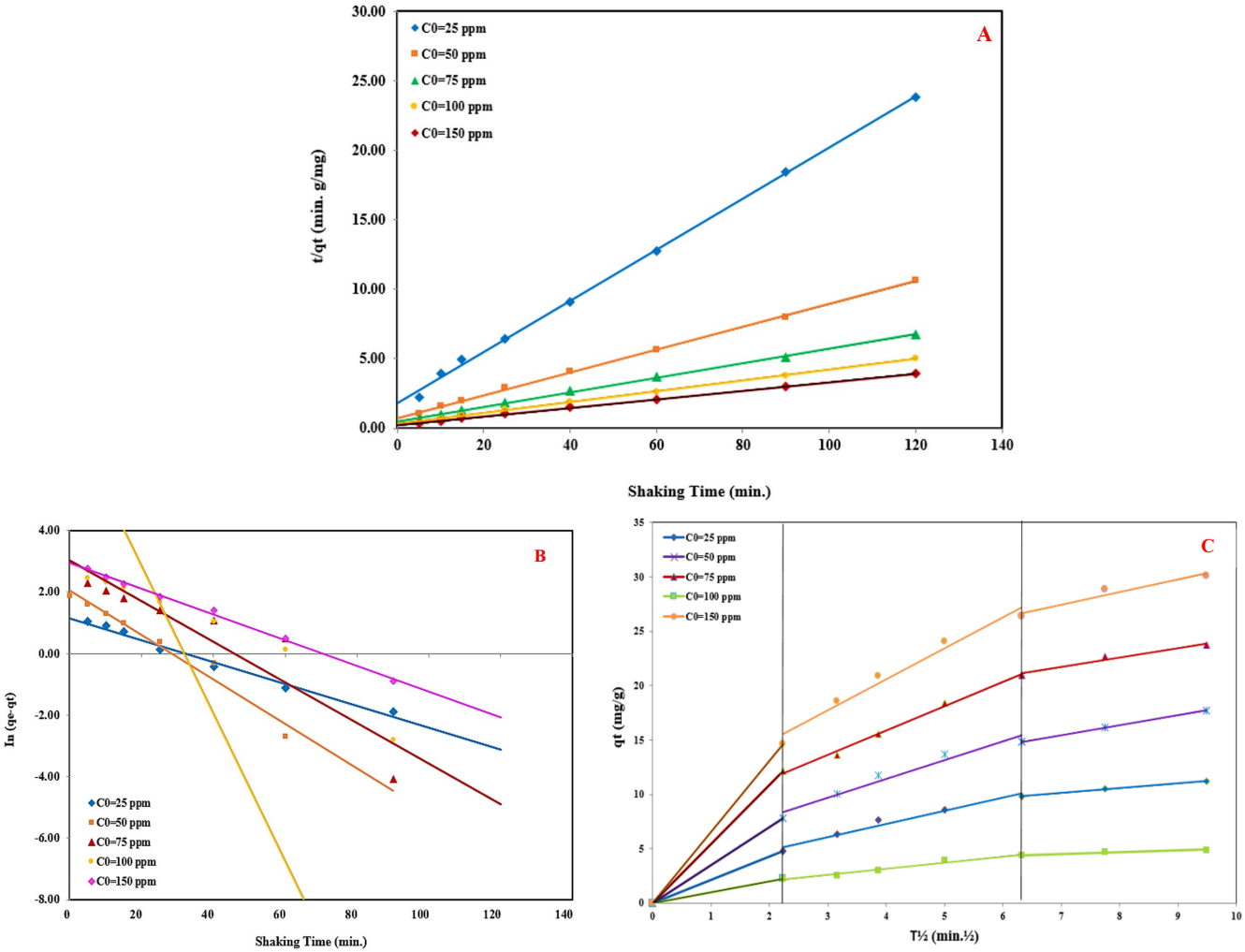

Figure 11. The kinetic models fitted to TEC adsorption.

$K_{2,des}$ is the 2nd order desorption rate constant ($g.mg^{-1}.min^{-1}$). Numerical integration over time was carried out iteratively for both rate expressions, as illustrated in Equation (14):

$$q_{n+1} = q_n - \left(\frac{dq}{dt}\right)_n (t_{n+1} - t_n) \quad (14)$$

where, q_0 denotes the initial concentration of TEC at time t_0 = 5 minutes, as determined from the preceding adsorption phase, while q_n represents the residual TEC concentration at time t_n. According to Equation (14), the TEC concentration (mg/g) at time t_{n+1} is obtained by subtracting the desorption rate multiplied by the time increment from the concentration at t_n.

As presented in Table 4, PSO model generally yielded higher correlation coefficients ($R^2 \geq 0.902$) compared to PFO model. Despite this, minimal differences were observed between the predicted (q_{n+1}) and experimental (q_n) values. Similar findings were reported by [60], who concluded that the modified PSO model provides a more accurate representation of desorption kinetics than its PFO counterpart.

3.5.3. Mechanism of TEC adsorption onto ZnO

ZnO exhibits amphoteric characteristics and has a point of zero charge (pH_{pzc}) around 7.5. This means that at pH values below 7.5, such as the acidic condition of pH of 5, the ZnO surface carries a net positive charge or shows amphoteric behavior allowing interactions with ionic species. At this pH, the ZnO surface can interact effectively with the zwitterionic form of tetracycline (TEC), which contains both positive and negative functional groups. Additionally, Zn^{2+} ions present on the ZnO surface can form coordination complexes with TEC molecules, further enhancing adsorption. Therefore, the adsorption of TEC on ZnO involves a combination of electrostatic interactions and surface complexation between TEC molecules and Zn^{2+} cations, leading to improved adsorption capacity, Figure 13.

3.5.4. Sorption isotherm

Adsorption is quantitatively characterized by isotherm models, which depict the equilibrium relationship between contaminant concentrations in the solid adsorbent and the liquid phase at a constant temperature, elaborate on the properties and type of adsorption as well as how the adsorbate interacts with the adsorbent [61]. When plotting the amount of adsorbate per unit mass of adsorbent (q_e) against the equilibrium concentration in solution (C_e), qe is observed to increase with C_e, though not in a strictly

Table 4. TEC desorption kinetic parameters.

Kinetic Model	Parameter	Cycle				
		1	2	3	4	5
Pseudo-first-order	q_n (mg/g)	9.4	9.028	5.5	7.5	6.1
	q_{n+1} (mg/g)	9.322	8.9527	5.4656	7.4219	6.049
	$K_{1,des}$ (min^{-1})	0.0023	0.0033	0.002	0.0032	0.004
	R^2	0.824	0.837	0.835	0.813	0.811
Pseudo-second-order	q_{n+1} (mg/g)	9.326	8.943	5.468	7.406	6.015
	$K_{2,des}$ (g/mg. min)	0.0003	0.0005	0.0004	0.0005	0.0009
	R^2	0.902	0.917	0.970	0.970	0.993

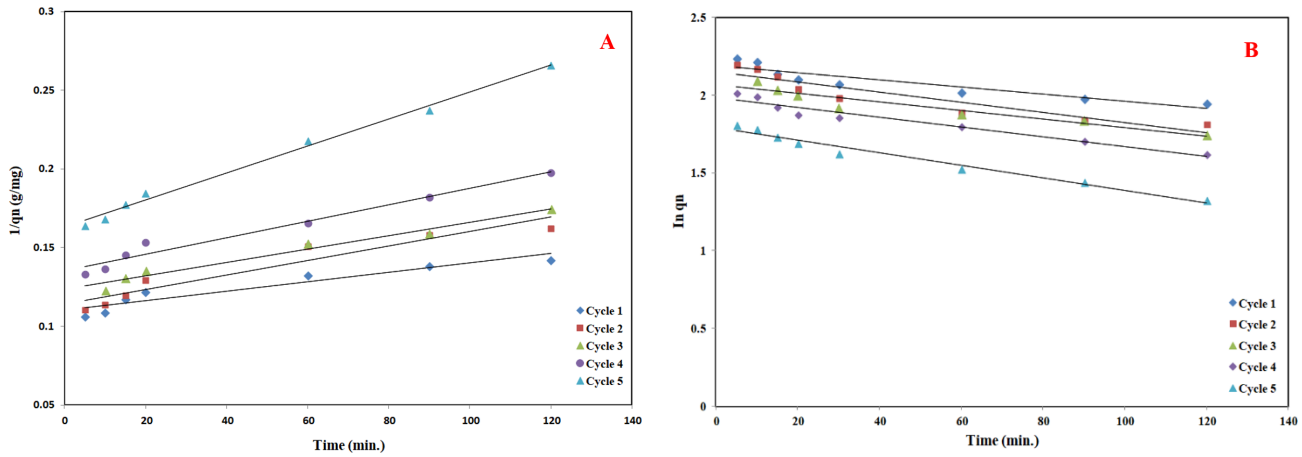

Figure 12. The kinetic of TEC desorption.

proportional manner [61]. The principal adsorption isotherm models are summarized as follow: The Langmuir model, developed in 1916 assumes that the adsorption process occurs at certain active sites localised to the adsorbent surface with all adsorption sites homogeneous in terms of energy [62], is as shown in Equation (15):

$$q_e = \frac{K_L . q_{max} . C_e}{1 + K_L . C_e} \quad (15)$$

where, q_e denotes the amount of adsorbate adsorbed at equilibrium (mg/g); q_{max} is the maximum sorbate uptake capacity (mg/g); K_L is the Langmuir isotherm constant (L/mg); and C_e represents the equilibrium concentration of sorbate in solution (mg/L). This model interprets adsorption data by assuming uniform sorption energies across the adsorbent surface and no interactions between adsorbed molecules at adjacent sites. Freundlich's model is as shown in Equation (16):

$$q_e = K_f . C_e^{(1/n)} \quad (16)$$

where, n and K_f representing the intensity and adsorption capacity, respectively.

Each parameters for isotherm model were determined by fitting the models to the experimental data. The corresponding sorption isotherms are illustrated in Figure 14, while all R^2 values are summarized in Table 5. Among the models, the Langmuir isotherm exhibited a higher R^2 compared to the Freundlich model. Nevertheless, both the sum of squared residuals (SSR) and the adjusted sum of squared residuals (ASSR) indicated a generally good agreement between the experimental and predicted values.

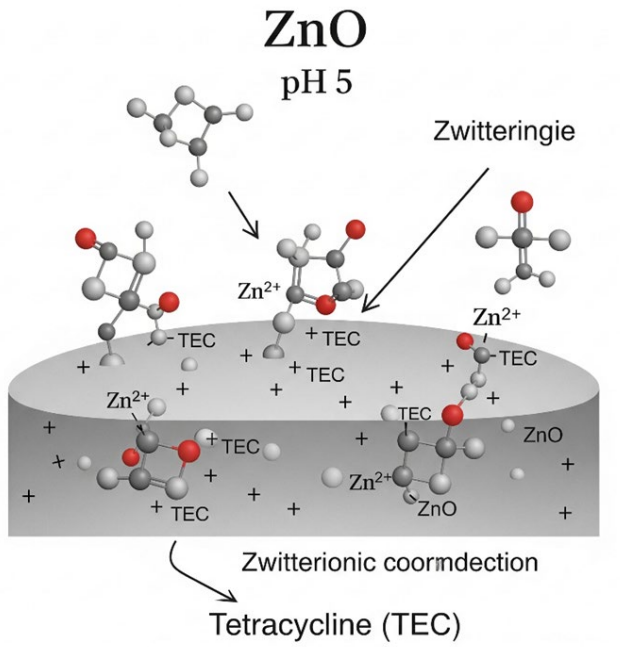

Figure 13. Schematic illustration of TEC adsorption onto ZnO.

3.6. Comparison Between Green-Synthesized and Commercial ZnO

The adsorption performance of the green-synthesized ZnO was compared with that of commercially available ZnO under identical experimental conditions. The results showed that the green-synthesized ZnO achieved a removal efficiency of 95%, while the commercial ZnO exhibited a slightly higher efficiency of 97%. This marginal difference indicates that the eco-friendly, plant-based synthesis route can yield ZnO nanoparticles with nearly comparable performance to the industrial material, while offering the added advantages of sustainability, non-toxicity, and the use of renewable resources. Therefore, the synthesized ZnO demonstrates its potential as a viable alternative to conventional ZnO for antibiotic removal (Figure 15).

4. Conclusions

In the present study zinc oxide nanoparticles were successfully synthesised using green tea leaves extract as caping and stabilization agent, characterized and then used to remove TEC antibiotic in aqueous solution. The zinc oxide structure and size were confirmed by SEM

Table 5. Parameters of Langmuir and Freundlich's model.

Langmuir		Freundlich	
q_{max} (mg/g)	110.56	K_f	4.91
K_L	0.0246	$1/n$	1.515
R^2	0.9984	R^2	0.9859
SSR	105.7687	SSR	122.8437
ASSR	0.1693	ASSR	1.7290
X^2	0.0763	X^2	0.7791
R_L	0.4481		

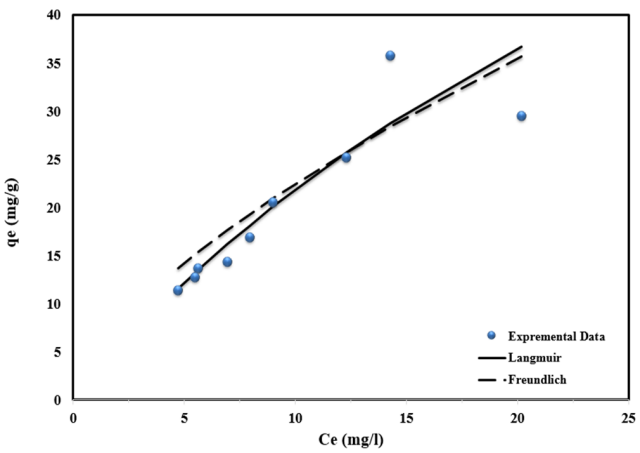

Figure 14. Isotherms of TEC adsorption onto ZnO.

analysis showed that the surface of ZnO exhibits a highly heterogeneous texture with irregular, rough surface and aggregated particles. XRD analysis proved the absence of any secondary phases or impurity peaks, indicating the high purity of the synthesized zinc oxide adsorbent. Tetracycline adsorption attained its peak capacity after 90 minutes of contact time. Highlighting the significant Effect of pH on adsorption efficiency. The adsorption mechanism of tetracycline onto ZnO NPs involves multiple sequential mechanisms. Also, the adsorption process was both spontaneous and feasible. Just a 31% reduction in adsorption efficiency was noted after five adsorption-desorption cycles. This study demonstrated that green synthesis of zinc oxide nanoparticles using tea leaves could be a suitable method for synthesizing an efficient adsorbent for sequestrating antibiotics from wastewater. Moreover, the potential use of this adsorbent in the area of real wastewater containing organic and inorganic materials and the potential challenges in scaling -up the synthesis of ZnO NPs should also be studied.

CRedit Author Statement

Author Contributions: Zahraa A. Abd Almjeed: Conceptualization, Methodology, Investigation, Resources, and Data Curation, Writing; Ahmed A. Mohammed: Conceptualization, Formal Analysis, Review and Editing, Supervision. All authors have read and agreed to the published version of the manuscript.

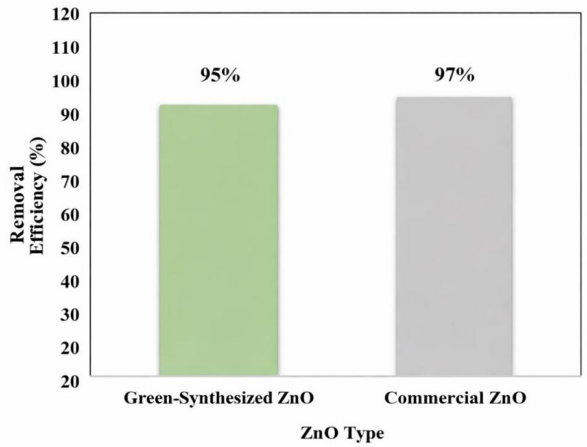

Figure 15. Comparison between efficiency of green-synthesized and commercial ZnO.

References

[1] ELmessaoudi, N., Mihy, Y., Singh, N., Gubernats, S., Fatima, R., Georgin, J., EL Mouden, A., Saghir, S., Kani, S ., Hwang, Y ., (2024). A critical review of Allura red removal from water : advancements in adsorption and photocatalytic degradation technologies and future perspectives. *Journal Environmental Chemical Engineering*, 12 (6), 114843. DOI: 10.1016/j.jece.2024.114843.

[2] Manyangadze, M., Chikuruwo, N.H.M., Narsaiah, T.B., Chakra, C.S., Radhakumari, M., Danha, G., (2020). Enhancing adsorption capacity of nano-adsorbents via surface modification: A review. *South African J. Chem. Eng*. 31, 25-32. DOI: 10.1016/j.sajce.2019.11.003.

[3] Hassani, A., Faraji, M., Eghbali, P. (2020). Facile fabrication of mpg-C3N4/Ag/ZnO nanowires/Zn photocatalyst plates for photodegradation of dye pollutant. *Journal of Photochemistry andPhotobiology A: Chemistry*, 400, 112665. DOI: 10.1016/j.jphotochem.2020.112665

[4] Hammood, Z.A., Mohammed, A.A. (2024) Adsorption of tetracycline CaMg Al- layer double hydroxide from an aqueous solution /red mud composite; kinetic, isotherm and thermodynamic. *Environmental Nanotechnology Monitoring & Studies Management*, 22, 101018. DOI: 10.1016/j.enmm.2024.101018

[5] Mansouri, F., Chouchene, K., Roche, N., and Kisibi, M., (2021). Removal of pharmaceuticals from water by adsorption and advanced oxidation processes : state of the art and trends . *Applied Science*, 11, 14, 6659. DOI: 10.3390/app11146659.

[6] Wang, X., Jing, J. Zhou, M., Dewil, R., (2023) Recent advanc in H2O-based advanced sewage oxidation processes for removal of antibiotics from wastewater, *Chin. Chem. Lett*. 34(3), 107621. DOI: 10.1016/j.cclet.2022.06.044.

[7] Kümmerer, K., (2009). Antibiotics in the aquatic environment–a review–part I. *Chemosphere*, 75(4), 417–434. DOI: 10.1016/j.chemosphere.2008.11.086

[8] Atiya, M.A., Mohammed, A.A., and Hussein, M.A. (2021). Extraction model to remove antibiotics from aqueous solution by emulsion and Pickering emulsion liquid membrane. *Desalination and Water Treatment*, 217, 262-271. DOI: 10.5004/dwt.2021.26826

[9] Alacahan, O.F., Ozyonar, F. (2024). Sound assisted electocoagulation. *Environmental Processes*, 11-58. DOI: 10.1007/s40710-024-00733-3.

[10] Mohammed, A.A., Mutar, Z.H., Al-Baldawi, I.A. (2021). Alternanthera spp. based-phytoremediation for the removal of acetaminophen and methylparaben at mesocosm-scale constructed wetlands. *Heliyon* 7 (11). DOI: 10.1016/j.heliyon.2021.e08403

[11] Mohsin, M.K., Mohammed, A.A. (2021). Catalytic ozonation for removal of antibiotic oxy-tetracycline using zinc oxide nanoparticles. *Applied Water Science*, 11(1). DOI: 10.1007/s13201-020-01333-w

[12] Balakrishnon, A., Chinthala, M., Pologoni, R., Vo, D., (2023). Removal of tetracycline from wastewater using g-C3N4 based photocatalysts: A review. *Environmental Research*. 216, Part 3, 114660. DOI: 10.1016/j.envres.2022.114660.

[13] Nie Y., Zhang T., Xu Y., Du Y., Ai J., Xu N. (2024). Study on mechanism of removal of sudden Tetracycline by compound modified biological sand filtration process. *J. Environmental Management*. 356, 120709. DOI: 10.1016/j.jenvman.2024.120709.

[14] Hassani, A., Pourshirband,N., Sayyar, P. (2025). Fenton and Fenton-like-based advanced oxidation processes. Innovative and Hybrid Advanced Oxidation Processes for Water Treatment, In: *Innovative and Hybrid Advanced Oxidation Processes for Water Treatment, Elsevier*. 171-203. DOI: 10.1016/B978-0-443-14100-3.00006-5

[15] Darvishi, A., Shafiee, G., Balajam, N.Z., Hemami, M.R., Ostovar, N., Heshmat, R. (2023). Cost-effectiveness analysis of sarcopenia management interventions in Iran. *BMC Public Health*, 23, 819. DOI: 10.1186/s12889-023-15693-w

[16] Hammood, Z.A., Mohammed, A.A. (2025). Understanding the sorbent properties of layered double hydroxide for the removal of pharmaceuticals from aqueous Solutions: A comprehensive review. *Results in Chemistry*, 13, 101952. DOI: 10.1016/j.rechem.2024.101952

[17] Aasli, B., ELMessaoudi, N., Miyah, Y., Benjelloun, M., Georgin, J., Franco, D.S., Hwang, Y., Lacherai, A. (2025). A comprehensive review of the use of urea - formaldehyde resin composites for the adsorption of organic and inorganic pollutants from water. *Nano-Structures and Nano Objects*. 43, 101495. DOI: 10.1016/j.nanoso.2025.101495.

[18] Muthukathija, M., sheik, M., Rama, V., (2023). Green synthesis of zinc oxide nanoparticles using Pisonia Alba leaf extract and its antibacterial activity. *Applied surface Science Advances*. 15, 100400. DOI: 10.1016/j.apsadv.2023.100400

[19] Jayachandran, A., Aswathy, T.R., Nairs, A.A. (2021) Green synthesis and characterization of zinc oxide nanoparticles using Cayratia pedata leaf extract. *Biochemistry and Biophysics Reports*. 26, 100995. DOI: 10.1016/j.bbrep.2021.100995.

[20] Al-darwesh, M.Y., Ibrahim, S.S., Mohammed M.A. (2024). A review on plant extract mediated green synthesis of zinc oxide nanoparticles and their biomedical applications *Results in Chemistry*, 7, 101368. DOI: 10.1016/j.carbpol.2013.12.074.

[21] Dhandapani, P., Siddarth, A.S., Kamalasckaran, S., Maruthamuthu, S., Rajagopal, G. (2014). Bio-approach ureolytic bacteria mediated synthesis of ZnO nanoparticles on cotton fabric and evaluation of their antibacterial properties. *Carbohydr. Polym*. 103, 448-455. DOI: 10.1016/j.carbpol.2013.12.074.

[22] Bhardwaj, K., Singh, K. (2023). Bio-waste and natural resource mediated eco-friendly synthesis of Zinc oxide nanoparticles and their photocatalytic application against dyes contaminated water. *Chemical Engineering Journal Advances*, 16, 100536. DOI: 10.1016/j.ceja.2023.100536.

[23] Irshad, M.A., Abdullah Latif, M., Nasim I; Nawaz R. Zahoor, A.F., Al-Mutairi, A.A., Al-Hussain, S.A., Irfan, A., Magdi, E., Zaki, A. (2024). Efficient chromium removal from. leather industrial wastewater in batch experimental study: Green synthesis and characterization of zinc oxide nanoparticles using Ficus benghalensis extracts. *Eco Toxicology and Environmental Safety*. 281, 11661. DOI: 10.1016/j.ecoenv.2024.116616.

[24] Cioanca, O., Lungu, I.I., Mita-Baciu, I., Robu, S., Burlec, A.F., Hancianu, M., Crivoi, F. (2024). Extraction and purification of catechins from tea leaves: an overview of methods, advantages, and disadvantages. *Separations*, 11(6), 171. DOI: 10.3390/separations11060171.

[25] Kader, D.A., Aziz, D.M., Mohammed, S.J., Maarof, N.N., Karim, W.O., Rashid, R.M., Ayoob, M.M., Qurbani, K. (2024). Green synthesis of ZnO / Catechin nanocomposite: comprehensive characterization, optical study, and computational analysis ,biological applications and molecular docking. *Materials Chemistry and Physics*, 319, 129408. DOI: 10.1016/j.matchemphys.2024.129408 .

[26] Jiehu, C., Chunlei, W., Ming, Z., Jie, Z., Li, F., Xiuhong, D., Leiming, C., Chunguang, L., (2020). 2D to 3D controllable synthesis of three Zn-Co-LDHs for rapid adsorption of MO by TEA-assisted hydrothermal method. *Applied Surface Science*, 534, 147564. DOI: 10.1016/j.apsusc.2020.147564.

[27] Aasli, B., EL Messaoudi, M., Mahmoudy, G., Miyah, Y., Erraji, F., Kanani, S., Lacherai, A. (2025) Synthesis of urea - formaldehyde resin at chitson composite for removal of congo red from an aqueous solution via adsorption: Box - Behnken design optimization. International Journal of Biological Macromolecules. 315, Part 2, 144648. DOI: 10.1016/j.ijbiomac.2025.144648.

[28] Wirunchit, S., Gansa, P., Koetniyom, W. (2021). Synthesis of ZnO nanoparticles by Ball-milling process for biological applications. *Materials Today: Proceedings*, 47, 3554-3559. DOI: 10.1016/j.matpr.2021.03.559

[29] Rathee, G., Kohli S., Chandra, R. (2020). Simultaneous elimination of dyes and antibiotic with a hydrothermally generated NiAlTi layred double hydroxide adsorbent. *ACS Omega*, 5, 2368 – 2377. DOI: 10.1021/acsomega.9b03785.

[30] Alwared, A.I., Mohammed, N.A., Al-Musawi, T.J., Mohammed, A.A. (2023). Solar-induced photocatalytic degradation Turquoise dyes using a titanium oxide/xanthan gum composite. *Sustainability*, 15(14), 10815. DOI: 10.3390/su151410815

[31] Busila, M., Musat, V., Alexandru, P., Romanitan, C., Brincoveanu, O., Tucureanu, V., Mihalache, I., Iancu, A.V., Dediu, V. (2023). Antibacterial and photocatalytic activity of ZnO/Au and ZnO/Ag nanocomposites. I*nternational Journal of Molecular Sciences*, 24(23), 16939. DOI: 10.3390/ijms242316939

[32] Naik, R., Nagaswarupa, H.P., Darukesha, B.H.M., Tejashwini, D.M. (2024). Characterization of Metal Oxide Nanomaterials. In Advances in *Space Radiation Detection: Novel Nanomaterials and Techniques* (pp. 37-57). Cham: Springer Nature Switzerland DOI: 10.1007/978-3-031-74551-5_3

[33] Pandey, P., Choubey, A.K. (2024). Green synthesized ZnO@ CuO nanocomposites using Achyranthes aspera leaves extract for dielectric applications. *Journal of Alloys and Compounds*, 970, 172492. DOI: 10.1016/j.jallcom.2023.172492

[34] Mohammed, A.A., Kareem, S.L. (2021). Enhancement of ciprofloxacin antibiotic removal from aqueous solution using ZnO nanoparticles coated on pistachio shell. *Desalin. Water. Treat.*, 213, 229-239. DOI: 10.5004/dwt.2021.26674.

[35] Alnasrawi, F.A., Mohammed, A.A. (2023). Enhancement of Cd2+ removal on CuMgAl-layered double hydroxide/montmorillonite nanocomposite: Kinetic, isotherm, and thermodynamic studies. *Arabian Journal of Chemistry*, 16(2), 104471. DOI: 10.1016/j.arabjc.2022.104471

[36] Alnasrawi, F.A., Mohammed, A.A., Al-Musawi, T.J. (2023a). Synthesis and application of layered double hydroxides as a superior adsorbent for the removal of hazardous contaminants from aqueous solutions: a comprehensive review. *Desalination and Water Treatment*, 297, 26-74. DOI: 10.5004/dwt.2023.29579

[37] Nava-Andrade, K., Carbajal-Arízaga, G.G., Obregón, S., Rodríguez-González, V. (2021). Layered double hydroxides and related hybrid materials for removal of pharmaceutical pollutants from water. *Journal of Environmental Management*, 288, 112399. DOI: 10.1016/j.jenvman.2021.112399.

[38] Holilah, Asranudin, EL M essaoudi, N., Ulfa, M., Hamzah, A., Abdul Hamid, Z.A., Ramadhani, D. V., Suryanegara, L., Maharika, M., Melenia, A. T., Pratama, A.W., Didik, P. (2024) Fabrication a sustaiinable adsorbent nanocellulose - mesoporous hectorite bead for methylene blue adsorption adsorption. *Case Studies in Chemical and Environmental Engineering*, 10, 100850. DOI: 10.1016/j.cscee.2024.100850.

[39] Mittal, J., (2021). Recent progress in the synthesis of Layered Double Hydroxides and their application for the adsorptive removal of dyes: a review. *Environ. Manage*. 295, 113017. DOI: 10.1016/j.jenvman.2021.113017.

[40] Alnasrawi, F.A., Mohammed, A.A., Al-Musawi, T.J. (2023). Synthesis, characterization and adsorptive performance of CuMgAl-layered double hydroxides/montmorillonite nanocomposite for the removal of Zn (II) ions. Environmental Nanotechnology, *Monitoring & Management*, 19, 100771. DOI: 10.1016/j.enmm.2022.100771

[41] Sharma, P., Kaur, R., Baskar, C., Chung, W., (2010) Removal of methylene blue from aqueous waste rice husk and rice husk ash. *Desalination and Water Treatment*, 259, 249-257. DOI: 10.1016/j.desal.2010.03.044.

[42] Mohammed, A.A., Kareem, S.L., Peters, R.J., Mahdi, K., (2022). Removal of amoxicillin from aqueous solution in batch and circulated fluidized bed system using zinc oxide nanoparticles: hydrodynamic and mass transfer studies. Environmental *Nanotechnology, Monitoring & Management*, 17, 100648. DOI: 10.1016/j.enmm.2022.100648.

[43] Hammood, Z.A., Mohammed, A.A. (2024). Enhanced adsorption of ciprofloxacin from an aqueous solution using a novel CaMgAl-layered double hydroxide/red mud composite. *Results in Engineering*, 23, 102600. DOI: 10.1016/j.rineng.2024.102600

[44] Ali, D.K., Mohammed, A.A. (2023). Optimization of adsorption parameters for pesticides removal using bentonite-layered double hydroxide by response surface methodology. *Desalination and Water Treatment*, 284, 87-100. DOI: 10.5004/dwt.2023.29282

[45] Zhuang, F., Yu, J., Ma, J., Chen, Z. (2017). Enhanced adsorption removal of antibiotics from aqueous solutions by modified alginate/ graphene double network porous hydrogel, *J. Colloid Interface Sci.*, 507, 250–259. DOI: 10.1016/j.jcis.2017.07.0339.

[46] Bao, J., Zhu, Y., Yuan, S., Wang, F., Tang, H., Bao, Z., Zhou, H., Chen, Y. (2018). Adsorption of tetracycline with reduced graphene oxide decorated with MnFe2O4 nanoparticles. *Nanoscale Research Letters*, 13, 1-8. DOI: 10.1186/s11671-018-2814-9

[47] Zhang, X., Lin, Y., He, Y., Chen, X., Luo, R., Shang, X., (2019). Study on adsorption of tetracycline by Cu-immobilized alginate adsorbent from water environment, *Int. J. Biol. Macromol.*, 124, 418–428. DOI: 10.1016/j.ijbiomac.2018.11.218.

[48] Mohammed, A.A., Al-Musawi, T.J., Kareem, S.L., Zarrabi, M., Al-Ma'abreh, A.M. (2020). Simultaneous adsorption of tetracycline, amoxicillin, and ciprofloxacin by pistachio shell powder coated with zinc oxide. *Arabian Journal of Chemistry*, 13 (3); 4629-4643. DOI: 10.1016/j.arabjc.2019.10.010.

[49] Zhang, Y., (2020). Magnetic Adsorbent Fe_3O_4/ZnO/LC for the Removal of Tetracycline and CongoRed from Aqueous Solution. *Molecules*, 28(18), 6499. DOI: 10.3390/molecules28186499

[50] Nurhasanah, I ., Gunawan, V., Sutanto, H. (2020) Cerium oxide nanoparticles application for rapid adsorptive removal of tetracycline in water, *J. Environ. Chem. Eng*., 8, 103613, DOI: 10.1016/j.jece.2019.103613.

[51] Saremi, F., Miroliaei, M.R., Nejad, M.S., Sheibani, H. (2020). Adsorption of tetracycline antibiotic from aqueous solutions onto vitamin B6-upgraded biochar derived from date palm leaves. *Journal of Molecular Liquids*, 318, 114126. DOI: 10.1016/j.molliq.2020.114126

[52] Song, Y.X., Chen, S., You, N., Fan, H.T., Sun, L.N. (2020). Nanocomposites of zero-valent Iron@ Activated carbon derived from corn stalk for adsorptive removal of tetracycline antibiotics. *Chemosphere*, 255, 126917. DOI: 10.1016/j.chemosphere.2020.126917

[53] Ahmadi, S.A.R., Kalaee, M.R., Moradi, O., Nosratinia, F., Abdouss, M. (2021). Core–shell activated carbon-ZIF-8 nanomaterials for the removal of tetracycline from polluted aqueous solution. *Advanced Composites and Hybrid Materials*, 4, 1384-1397. DOI: 10.1007/s42114-021-00357-3

[54] Nasiri, A., Rajabi, S., Amiri, A., Fattahizade, M., Hasani, O., Lalehzari, A., Hashemi, M. (2022). Adsorption of tetracycline using CuCoFe2O4@ Chitosan as a new and green magnetic nanohybrid adsorbent from aqueous solutions: Isotherm, kinetic and thermodynamic study. *Arabian Journal of Chemistry*, 15(8), 104014. DOI: 10.1016/j.arabjc.2022.104014

[55] Da, J.I., Meng, X., Zhang, Y., Huang, Y. (2020) . Effects of modification and magnetization of rice straw derived biochar on adsorption of tetracycline from water, *Bioresour. Technol*., 311 123455. DOI: 10.1016/j.biortech.2020.123455.

[56] Ren, Z., Zha, J., Li, N., Zhou, P., Wang, F., Wang, L., Liang, J. (2023). Removal performance and mechanism of tetracycline hydrochloride in aqueous by geopolymers from tourmaline tailings. *Journal of Environmental Chemical Engineering*, 11(5), 111034. DOI: 10.1016/j.jece.2023.111034

[57] Sulaymon, A.H., Mohammed, A.A., Al-Musawi, T.J. (2014).Comparative study of removal of cadmium and Chromium ions from aqueous solution using low - cost biosorbent . *International Journal of Chemical Reactor Engineering*. 12, (1), 1-10. DOI: 10.1515/ijcre-2014-0024.

[58] Mohammed, A.A. (2015). Biosorption of lead, cadmium, and zinc onto sunflower shell: equilibrium, kinetic, and thermodynamic studies. *Iraqi Journal of Chemical and Petroleum Engineering*, 16(1), 91-105. DOI: 10.31699/IJCPE.2015.1.9

[59] Birungi, Z., Chirwa, E.M.N., (2015). The adsorption potential and recovery of thallium using green microw - algae from eutrophic water sources. *Journal of Hazardous Material*, 299, 67-77. DOI: 10.1016/j.jhazmat.2015.06.011.

[60] Njikam, E., Schiewer, S. (2012). Optimization and kinetic modeling of cadimum desorption from citrus peels: A process for biosorbent regeneration. *Journal of Hazardous Materials*, 213, 242–248. DOI: 10.1016/j.jhazmat.2012.01.084.

[61] Mohammed, A.A., Alnasrawi, F.A. (2024). Cadmium sequestration with MgCuAl-layered double hydroxide@ montmorillonite nanocomposite in batch and circulated fluidized bed column Experiments. *Desalination and Water Treatment*, 100744. DOI: 10.1016/j.dwt.2024.100744

[62] Kamar, F.H., Nechifor, A.C., Mohammed, A.A., Albu, C.P. (2015). Removal of lead and cadmium ions from aqueous solution using walnut shells as low-cost adsorbent material. *Revista de Chimie (Bucharest)*, 66(5), 615–620.: https://bch.ro/pdfRC/FIRAS%20H%20K.pdf%205%2015.pdf.